UNITED KINGDOM INFRARED TELESCOPE'S SPECTROGRAPH OBSERVATIONS OF HUMAN-MADE SPACE OBJECTS

Brent Buckalew[(1)]
Kira Abercromby[(2)]
Susan Lederer[(3)]
James Frith[(4)]
Heather Cowardin[(4)]

[(1)]*JACOBS, 2224 Bay Area Blvd. Houston, TX 77058 USA, brent.a.buckalew@nasa.gov*
[(2)]*California Polytechnic State University, San Luis Obispo, kabercro@calpoly.edu*
[(3)]*NASA JSC, 2101 NASA Parkway, XI411, Houston, TX 77058 USA, susan.m.lederer@nasa.gov*
[(4)]*JACOBS JETS, University of Texas El Paso, 2224 Bay Area Blvd. Houston, TX 77058 USA*

ABSTRACT

Presented here are the results of the United Kingdom Infrared Telescope (UKIRT) spectral observations of human-made space objects taken from 2014 to 2015. The data collected using the UIST infrared spectrograph cover the wavelength range 0.7-2.5 μm. Overall, data were collected on 18 different orbiting objects at or near the geosynchronous (GEO) regime. Thirteen of the objects are spacecraft, one is a rocket body, and four are cataloged as debris pieces. The remotely collected data are compared to the laboratory-collected reflectance data on typical spacecraft materials; thereby general materials are identified but not specific types. These results highlight the usefulness of observations in the infrared by focusing on features from hydrocarbons and silicon. The spacecraft show distinct features due to the presence of solar panels. Signature variations between rocket bodies, due to the presence of various metals and paints on their surfaces, show a clear distinction from those objects with solar panels, demonstrating that one can distinguish most spacecraft from rocket bodies through infrared spectrum analysis. Finally, the debris pieces tend to show featureless, dark spectra. These results show that the laboratory data in its current state give excellent indications as to the nature of the surface materials on the objects. Further telescopic data collection and model updates to include more materials, noise, surface roughness, and material degradation are necessary to make better assessments of orbital object material types. A comparison conducted between objects observed previously with the NASA Infrared Telescope Facility (IRTF) shows similar materials and trends from the two telescopes and from the two distinct data sets. However, based on the current state of the model, infrared spectroscopic data are adequate to classify objects in GEO as spacecraft, rocket bodies, or debris.

1. INTRODUCTION

One of the roles of the NASA Orbital Debris Program Office at Johnson Space Center (JSC) is to characterize the debris environment through the assessment of the physical properties (type, mass, density, and size) of objects in orbit. Knowledge of the geosynchronous orbit (GEO) debris environment, in particular, can be used to determine the hazard probability at specific GEO altitudes and aid predictions of the future environment. Currently, an optical size is calculated using an assumed albedo for an object and its intensity measurement. However, identification of specific material type or types could improve albedo accuracy and yield a more accurate size estimate for the debris piece. Using spectroscopy, it is possible to determine the surface materials of space objects.

2. DATA COLLECTION AND REDUCTION

2.1 Telescope Observations

Observations of orbital objects were taken with the 3.8-meter telescope at the United Kingdom Infrared Telescope (UKIRT) using the UKIRT 1-5 micron Imager Spectrometer (UIST) [1] instrument on 17-26 March 2015, 9-14 April 2015, 16-17 April 2015, 20-21 April 2015, and 24-27 April 2015. UIST was used in spectroscopy mode, and the slit width was 4 pixels (~0.48″). The data from the nights reported herein were spectrophotometric. In this configuration, the instrument provides a spectral resolution ($\lambda/\Delta\lambda$) of 320 for the IJ (0.862-1.418 microns) grism, of 450 for the JH (1.127-1.903 microns) grism, and of 500 for the HK (1.395-2.506 microns) grism. Signal-to-noise values of the data obtained are contingent on the brightness of the object at the time of observation, the total integration time, and the atmospheric conditions at the summit. The signal-to-noise values for most objects observed with this instrument are attainable in excess of 100, given good viewing conditions.

Over the course of these observations, spectral data were acquired on a subset of cataloged GEO targets from the U.S. Space Surveillance Network (SSN) database. These objects included spacecraft, rocket bodies, and orbital debris (see Table 1 for a summary of all observations). In two cases, SSN 14234 and SSN 27400, were observed in both March and April 2015. In ten cases, individual objects were observed on multiple nights in the same month. During the course of a night's observation campaign, calibration data were acquired including flats, arc lamps (wavelength calibration), atmospheric standards (telluric feature removal), and solar analogs (for relative reflectance ratios). Typically, exposure time sets for the SSN objects were 60 seconds placed in five pairs

(for a total of 10 exposures), where the object was shifted 1" up and down the slit (necessary for sky emission removal and bias/dark removal) for a given slit pair.

Table 1. UKIRT UIST Observation Summary

SSN	Common Names	International Designator	17-26 March 2015	9-14, 16-17, 20-21, & 24-27 April 2015
08832	TITAN 3C TRANS TAGE DEB	1976-023J		X
11669	OPS 6393 (FLTSA TCOM 3)	1980-004A		X
12855	SBS 2	1981-096A		X
13431	ANIK D-1	1982-082A		X
14234	ARABS AT 1DR (TELST AR 3A)	1983-077A	X	X
14341	SL-4 Debris	1983-097C		X
15383	ARABS AT 1-D (ANIK D-2)	1984-113B		X
15385	SPACE NET 2	1984-114A		X
16274	MOREL OS 2	1985-109B		X
19751	COSMO S 1989 (ETALO N 1)	1989-001C		X
20026	COSMO S 2024 (ETALO N 2)	1989-039C		X
20558	ASIASA T 1	1990-030A		X
20570	NEWSA T-1 (PALAP A B2R)	1990-034A		X
21648	COSMO S 2054 DEB	1989-101G		X
23185	APSTA R1	1994-043A	X	
23615	IUS R/B (2)	1995-035D		X
27400	ASTRA 3A	2002-015B	X	X
39886	SL-16 DEBRIS	1993-016BL	X	

The data were reduced using Starlink [**3**]. The typical settings used were to recalibrate the data in our office using orac-dr followed by the steps outlined in [4].

Once the steps above were completed, the relative reflectance ratio spectra of the objects were produced. These images were produced by ratioing the object and solar analog star. To insure sky conditions are completely removed from the image, both the object spectra and solar analog spectra were ratioed by the standard star spectra closest in time and position to the object observations. This procedure gives us a final ratio of the SSN to solar analog where the atmospheric lines have been eliminated completely. An example of this ratio can be found in Figure 1.

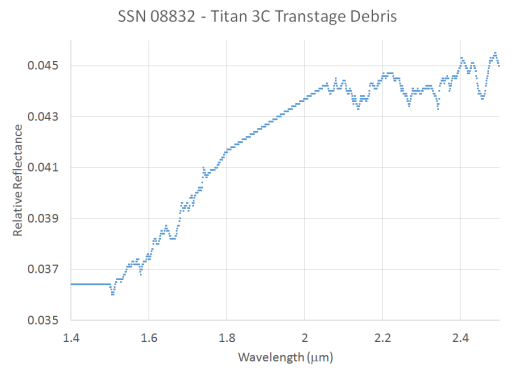

Figure 1. SSN 8832 spectral data acquired 13 April 2015 ratioed to the solar analog star SA 107-684. The y-axis is relative reflectance, and the x-axis is wavelength in microns. The smooth lines (e.g., between 1.8 and 2.0 μm) are indicative of the removal of the residuals left over from removing telluric features. The removal of these features aided with the running of the material deduction software.

2.2 Laboratory Data

When collecting data in a laboratory, a white reference is measured and compared to the material spectrum such that the resulting spectrum is called an absolute reflectance measurement that is on the scale of zero to one. However, there is not such an absolute reflectance standard at the same distance and orientation of each of the satellites. Therefore, the data are considered as relative reflectances. In these cases, the shape of the spectrum and the location and strength of the absorption features are used to determine material and not the percent reflectivity. To be able to compare measurements from two different objects, it may be necessary to scale to the object's reflectance so that both reflectances fit on one plot. When this practice was done, it will be noted.

An Analytical Spectral Device field spectrometer that has a wavelength range from 0.3 to 2.5 microns (μm) with a resolution of 10 nanometers at a wavelength of 2 μm and 717 channels was used to obtain the laboratory measurements. From these laboratory measurements, a database of more than 300 common spacecraft materials reflectance spectra was assembled and is used for comparison with the IRTF remote observations to determine material type [5]. All of the laboratory data referred to on the figures in this paper are from the NASA Spectral Database [5].

For these comparisons, the objects were known, catalogued pieces and thus the authors had *a prior* knowledge as to what materials would be best to include when comparing the remote data to lab data. However, some non-traditional materials were included as well such that the list is shown in Tab. 2. All of the solar cells are different in type; not all the types are known and those that are not known are typed generically. The exposed white paint is white paint that was flown on the Long Duration Exposure Facility; the paint turned a gold color with exposure to the environment [5].

Table 2. List of Materials for Comparison

Material		
Solar Cell Montana (MT)	Inconel (nickel-chromium superalloy)	Carbon Epoxy
Solar Cell Polysat	Anodized Aluminum	White Paint
Solar Cell at 0° phase	Aluminum Beta Cloth	Exposed White Paint
Solar Cell TRMM	Aluminized Kapton	Multi-Layer Insulation—Kapton

3. SPECTRAL UNMIXING

Spectral unmixing is the process of inverting material proportions from a combined spectrum that has distinct components that are linearly mixed. Rapp [6] developed a Constrained Linear Least Squares (CLLS) model with the application of unmixing reflectance spectral data of orbiting objects. Spectra are added linearly according to the proportion represented on the surface of the object. Considering orientation of incident light and the object, the full equation defining the combined spectrum in terms of orientation [6, 7] is:

$$S_{combined} = \sum_{i=1}^{n} p_i B_i S_i + N \quad (1)$$

where S is a spectrum, i is an index representing the i^{th} material, p is the material proportion of the full spectrum, N is noise, and B_i is the orientation coefficient for the i^{th} material. Equation 1 is still an approximation, however, as the orientation can change the spectrum. It should be noted that $S_{combined}$ and S_i can be represented as very long vectors, with reflectance values at each of the measured wavelengths. This allows an expansion into a vector math representation:

$$\vec{S}_{combined} = p_1 B_1 \overrightarrow{S_1} + \cdots + p_n B_n \overrightarrow{S_n} + \vec{N} \quad (2)$$

where p_i and B_i are both scalars, making it quite easy to restate this as a matrix multiplication problem with a known solution:

$$S_c = SA. \quad (3)$$

Unfortunately, the matrix S is not square so it cannot be truly inverted to solve directly for A so a pseudo-inverse can be used. When applied to this problem this inverse is known as a least-squares optimization:

$$S^T S_c = S^T SA \quad (4)$$

Multiplying both sides by S^T creates a square matrix that is guaranteed to be invertible:

$$(S^T S)^{-1} S^T S_c = A \quad (5)$$

This function minimizes Equation 5 and provides a beginning point for the solution to the unmixing problem. Testing this solution, for some combined spectra the unmixer returned negative proportion values, which is physically impossible. This is because the model is trying to match shape and subtracting materials can be the same as adding in terms of the final result. To rectify this issue a constrained least squares function was used, MATLAB's built in *lsqnonneg* function. The function uses a modified Lagrange multiplier method to solve the constrained problem. By reframing this as a vector problem, and recognizing it as a minimization problem, it becomes clear that the Lagrange solution is solving the constrained minimization problem:

$$f = (S_c - SA) \;\; A \geq 0 \quad (6)$$

This is solved for the specific $A \geq 0$ case by the *lsqnonneg* function. To maintain the constraint using a Lagrange multiplier method, the function first calculates the least squares solution, including negative solutions. It then uses those solutions to create a vector of logicals defining which solutions are negative, and need to be corrected. This vector becomes the Lagrange multiplier, and the optimization is performed. This process is repeated until an optimum solution is found.

To estimate the error in the results when unknown spectra are unmixed, the difference between the original and

unmixed spectra is calculated (called the residual). Since a vector approximation method is used to calculate the best unmixing solution, the norm is calculated, and used for error. This area is then used to calculate the error based on the difference in area.

$$E = \frac{Norm_{diff}}{Norm_{orig}} = \frac{\sqrt{S_{diff}^T S_{diff}}}{\sqrt{S_c^T S_c}} \quad (7)$$

This error estimation gives a percentage error, and gives an estimation of the cut-off point of significant figures in the output. This model takes all the materials supplied and creates the best, combined spectrum based on the above method.

4. RESULTS

The remotely collected data are compared to the laboratory-collected reflectance data on typical spacecraft materials; thereby general materials are identified but not specific types. Each spectral image shown contains the remote data on the object and the spectral unmixing program (CLLS) spectrum. In addition, a simple subtraction between the two spectra is also shown on the plots. This difference is calculated at each wavelength. The overall error (shown in the calculations in the previous section) is listed in the figure captions.

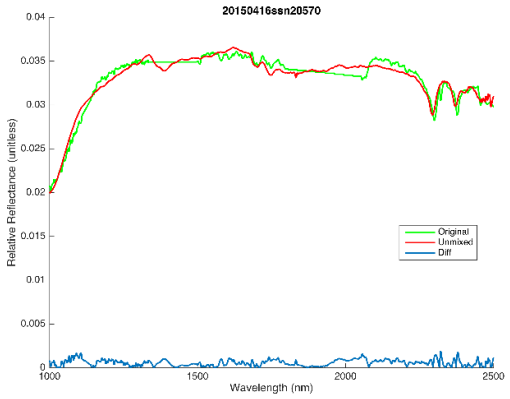

Figure 2. Spectral Data over the IJ and HK grisms from SSN20570. Green line is the original data, red line is the model fit to the data, and blue is the difference between the green and red lines. Each grism result was modeled separately. The percent error is 1.7% for IJ and 1.8% for HK. The largest variations occur around the water features and the organic features.

Figure 3. Palapa-B image. This is an artist rendition of a HS 376 communication satellite. Ref: http://space.skyrocket.de/doc_sdat/palapa-b.htm.

Spectral data on object SSN20570 (NEWSAT-1 [PALAPA B2R]) is shown in Fig. 2. The spectral data from the IJ grism and HK grism are plotted on the same figure. Both model data and the remote data are scaled such that their reflectances are compared. The matching materials used in CLLS were multi-layered insulation (MLI), solar cell, anodized aluminum, Inconel, white paint, and exposed white paint. The model fits the original data to 1.7% for the IJ grism and 1.8% for the HK grism. This error is typical of the data presented. Solar cells have a band gap feature near 1100 nm, as seen in the original and unmixed data in Fig. 2. These results are consistent with the satellite design, which is a cylindrical bus-type covered in solar cells, similar to Fig. 3.

In addition to the solar cell feature, common features due to carbon-hydrogen (C-H) are seen near 1700 nm and 2400 nm in both the CLLS model and remote data. The laboratory data tend to have some of the water features present (seen in Fig. 2 near 1400 and 1900 nm); however, the remote data have them completely removed due to the amount of water in the atmosphere. This removal makes it difficult to assess when the water features are due to the atmosphere and when they are from the spacecraft. Therefore, the features are removed completely such that an erroneous statement of water being present is not made. Thus, those regimes will never agree with the CLLS model in any of the figures shown. In future work, the intent is to remove the features from the laboratory data and redo the comparison.

Object SSN21648 (COSMOS 2054 Debris) did not compare well to the CLLS model. As shown in Figure 4, the spectral data is for the IJ grism. The data are effectively flat with no obvious absorption features; the majority of debris spectra seen in this study and within the study using Infrared Telescope Facility data [8] are similar. The percent error for this fit of the 21648 data is 10.6%. Currently, the spectral library of materials has no information on ejected materials from satellites due to explosions or collisions. More material information is necessary to give any material identification from actual orbital debris.

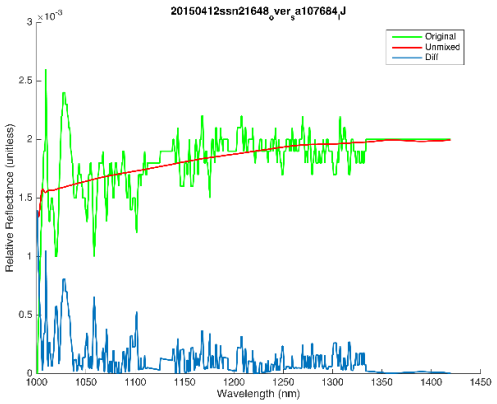

Figure 4. Spectral Data from SSN21648 with the IJ grism. Green line is the original data, red line is the model fit to the data, and blue is the difference between the green and red lines. The percent error is 10.6%. Debris typically have a flat composition. The spectral library of materials currently does not have the necessary knowledge to deal with these objects.

The CLLS had the hardest time matching materials with the orbital debris pieces. Three of the four debris pieces had some of the worse fits based on percentage errors. The CLLS model did not have materials in the database to match the debris pieces. For the COSMOS 2054 Debris, aluminum was the dominant match. In fact, SSN08832 (Titan Transtage 3C Debris), SSN 14341 (SL-4 Debris), and SSN 39866 (SL-16 Debris) all had fits with aluminum as a dominant material. In some cases (e.g., 12 April HK spectra of SSN08832), the materials fit with the CLLS model contain a contribution of solar cell emission. The authors think that solar panels are not in these objects, but some material with similar spectral response that is not in the database and model is present in the relative reflectance spectra.

The best fit spectra was that for the HK grism data of SSN 16274 (MORELOS 2). MORELOS 2 is a HS 376 like that depicted in Fig. 3. The fit for the MORELOS data is found in Fig. 5. The percentage error is 0.008% for the data taken on 24 April and 0.01% for the data taken on 16 April. Several of the key points discussed with the spectra of NEWSAT-1 can be reiterated here. Please see above for the prominent features discussed.

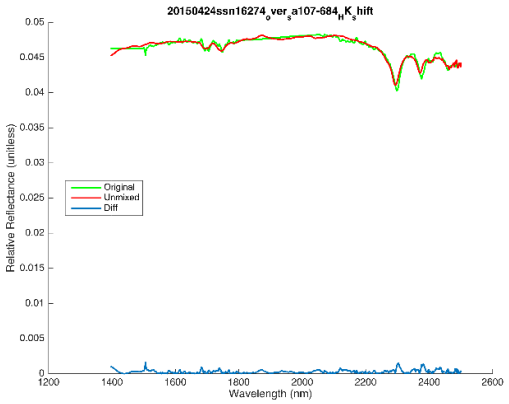

Figure 5. Spectral Data from SSN16274 with the HK grism. Green line is the original data, red line is the model fit to the data, and blue is the difference between the green and red lines. The percent error is 0.008%. This spectra and the features are similar to those found in Fig. 2.

The results of the one rocket body, SSN23615, are shown in Fig. 6. SSN23615 is an Inertial Upper Stage (IUS) rocket body and is shown in Fig. 7. Four spectra were taken of this object on 17 and 20 April. The JH grism was observed on both nights. The CLLS model was able to detect the C-H features and the general slope to within 3.2%, 3.8%/5.2%, and 2.7% for the IJ, JH, and HK grism spectra. While solar cells are not found on the rocket body, the HK grism and IJ grism results are best with a solar cell as one of the components. Fig. 7 shows the entire rocket body and not just the final stage that resides in GEO. That stage may display significant properties of Kevlar (motor case) and carbon/carbon (nozzle). Neither material is represented in the current material database. Thus, the solar cells, while not accurate, could be a stand in for these other materials.

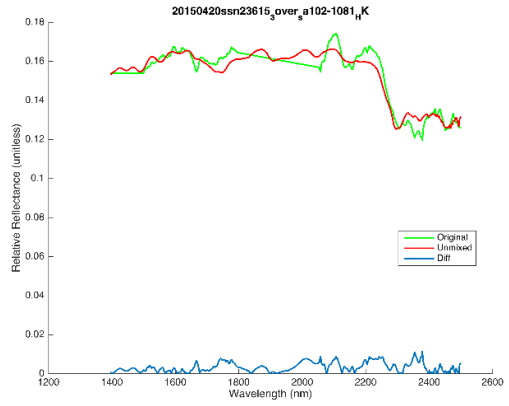

Figure 6. Spectral Data from SSN23615 with the HK grism. Green line is the original data, red line is the model fit to the data, and blue is the difference between the green and red lines. The percent error is 2.7%.

Rocket bodies should not have solar cells. However, in this fit along with the fit for the IJ grism, a model using solar cells works the best. The JH fits were best without solar cells.

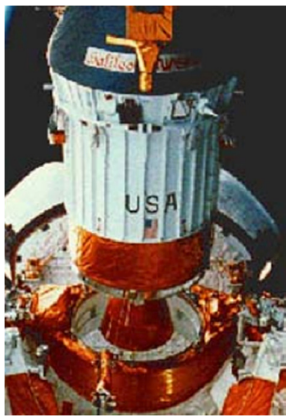

Figure 7. IUS rocket body (photo credit: NASA.gov)

Overall, the CLLS model showed promising results. Since all of the images could not be shown in the paper, a review of the materials identified and the percent error is shown in Tab. 3. The dominant material found was solar cells. The debris objects had higher error values showing that the model does not contain the materials shown in the remote sample. The differences between the results between an intact spacecraft, rocket body, and debris piece are evident by the material selected.

4.1 Single Order versus Stitched Spectra

What one is supposed to do with the 3 grism spectra is to stitch the 3 orders together to form a continuous spectra. It is possible that a full spectrum gives a more complete understanding of the material properties of these objects. We plot SSN 16274 results in Fig. 8 for comparison with those of Fig. 2. The results in Fig. 8 are a stitched spectra from data from a single night. The stitched spectra in this case has a higher percentage error, 0.01%, than the best fit from an individual order of the same object, 0.008%. In a comparison of the percentage errors of the individual order fits for an object to the percentage errors of the stitched spectra, the individual order fits have a factor of two smaller percentage errors than the percentage errors of the fits of the stitched spectra.

We also have the additional ability to average over several months of observations. The two objects, SSN16274 and SSN 27400, were both successfully fit with a one night and multiple night stitches. The multiple night stitches in both cases produced a fit with a worse percentage error but only by an increase of 1%. For SSN16274, this increase is from 0.01% to 1%. For SSN27400, this increase is from 9% to 10%.

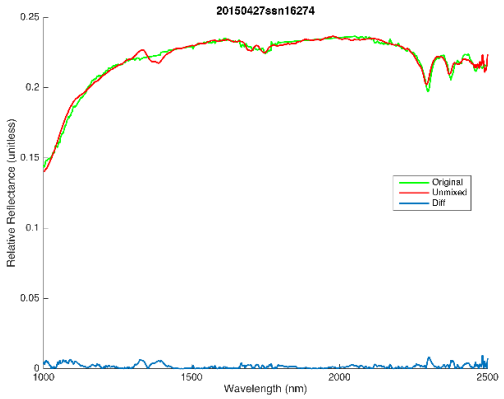

Figure 8. Spectral Data from SSN16274 that stitches the 3 grisms together. Green line is the original data, red line is the model fit to the data, and blue is the difference between the green and red lines. The percent error is 0.01%. From Fig. 2, that this percentage error is similar to the percentage error of this stitched spectra.

4.2 Comparison to Previous Study That Used NASA Infrared Telescope Facility Data

[8] is a previous study that used the same model but with NASA Infrared Telescope Facility (IRTF) data. Both studies were infrared based and both studies observed similar (sometimes the exact) objects. IRTF is one continuous spectra without the various grism orders like the UKIRT data. Despite these data differences, the model fits both sets of data well. The percentage error range of their fits was 1%—9%. Eight objects were observed and modeled in this study and in [8]. Seven of the eight objects have similar model composition results and similar percentage errors. The model composition of our study seems to have more materials. This result can be most easily explained by the increase in spectral resolution achieved with UKIRT compared to IRTF. SSN21648, debris, has more material components in the IRTF result compared to the UKIRT result. The percentage error of the fit model is higher in the UKIRT study, 10%, than the error in the IRTF study, 1%.

5. CONCLUSIONS

Spectral data taken at UKIRT during 2015 were shown and compared to a constrained linear least squares model using common spacecraft materials. The data collected using the UIST infrared spectrograph cover the wavelength range 0.7-2.5 μm. With UIST data, one can achieve a greater spectral resolution to identify narrower spectral features associated with materials. Overall, data were collected on 18 different orbiting objects at or near the GEO regime. Four of the objects were debris pieces, one was a rocket body, and thirteen were spacecraft.

The dominant material found was solar cells. The majority of the debris objects had higher error values showing that the model does not contain the materials shown in the remote samples. Like the conclusions of [8], the materials used to identify debris, spacecraft, and rocket bodies do differ. When using UIST data for material identification, we recommend that data be used to fit 1 spectral grism, HK, for identification. From this one grism, one can get sufficient spectral coverage and a decent model fit (based on our percentage errors in Tab. 5).

Future work on this topic includes adding more noise to the model such as surface roughness, examining the phase angles in conjunction with the spectra, and adding more laboratory materials to the model in hopes of more clearly defining the material types of these objects. Due to the wide variation of materials used on spacecraft, coatings applied to those materials, and space environmental effects while on orbit, having a perfect match between laboratory data and remote data would be impossible. However, the inclusion of more materials into the model and including space environmental and material degradation effects as well will increase the likelihood of determining the material types of these orbiting objects.

6. ACKNOWLEDGEMENTS

UKIRT acknowledgement here.

7. REFERENCES

1. Ramsay Howat S.K., *et al.*, 2004, "The commissioning of and first results from the UIST imager spectrometer", In Proc Spie 5492, UV and Gamma-Ray Space Telescope Systems, eds. Hasinger G, Turner M.J., p. 1160
2. Abercromby, K.J., *et al.*, Reflectance Spectra Comparison of Orbital Debris, Intact Spacecraft, and Intact Rocket Bodies in the GEO Regime, *European Conference on Space Debris*, April 2009.
3. Currie, M. J. et al., Starlink Software in 2013, Astronomical Data Analysis Software and Systems XXIII. Proceedings of a meeting held 29 September – 3 October 2013 at Waikoloa Beach Marriott, Hawaii, USA. Edited by N. Manset and P. Forshay ASP conference series, vol. 485, 2014, p. 391
4. http://www.ukirt.hawaii.edu/observing/cookbooks/spectroscopy_reduction_cookbook.html
5. NASA JSC Spacecraft Materials Spectral Database, NASA JSC, 2004.
6. Rapp, J., Identification of Orbital Objects by Spectral Analysis and Observation of Space Environment Effects, Master's Thesis, California Polytechnic State, San Luis Obispo, September 2012.
7. Keshava, N. and Mustard, J. F., Spectral Unmixing. *IEEE Signal Processing Magazine* , 44-57, January 2002.
8. Abercromby, K., Buckalew, B., Abell, P., and Cowardin, H. *Proceedings of the Advanced Maui Optical and Space Surveillance Technologies Conference*, 2015.

Table 3: Details of the material matches for the objects observed

Date (YYYYMMDD)	SSN	Common Name	Materials (in order)	Percentage Error	Type	Grism Fit
20150412	08832	TITAN 3C TRANSTAGE DEBRIS	Anodized Aluminum, less than 1% of solar cell MT, ITO Kapton, Exposed White paint, White paint, Kapton	1.5%	debris	HK
20150412	08832	TITAN 3C TRANSTAGE DEBRIS	Inconel, GPS Zero Phase, Solar Cell CP	7.0%	debris	IJ
20150413	08832	TITAN 3C TRANSTAGE DEBRIS	White Paint, Anodized Aluminum, Solar Cell MT, Beta Cloth	1.1%	debris	HK
20150413	08832	TITAN 3C TRANSTAGE DEBRIS	Kapton (Al), Inconel, GPS Zero Phase, AL 1100, Solar Cell MT and CP	1.9%	debris	IJ
20150414	11669	FLTSATCOM F3	GPS Zero Phase, Al 1100, Inconel, Kapton, White Paint	1.6%	satellite	HK
20150414	11669	FLTSATCOM F3	GPS Zero Phase, Inconel, Solar Cell MT, Solar 15, Kapton, AL 1100	1.9%	satellite	IJ
20150420	11669	FLTSATCOM F3	Anodized Aluminum, White Paint, Al, Exposed White Paint, Kapton (ITO), Solar Cell MT	0.1%	satellite	HK
20150420	11669	FLTSATCOM F3	Solar Cell MT, Anodized Aluminum, Inconel, White Paint	3.8%	satellite	JH
20150421	12855	SBS 2	GPS Zero Phase, Beta Cloth, Anodized Aluminum, Solar 15, Solar Cell MT, White Paint	1.3%	HS 376	HK
20150421	12855	SBS 2	GPS Zero Phase, Solar Cell MT, Inconel, Al 1100, White Paint, Kapton	2.4%	HS 376	IJ
20150421	13431	ANIK D-1	Anodized Aluminum, GPS Zero Phase, Solar 15, Solar Cell MT, Exposed White Paint, White Paint	1.2%	HS 376	HK
20150421	13431	ANIK D-1	GPS Zero Phase, Inconel, Solar Cell CP, Solar Cell MT, Al 1100, White Paint, Solar 15	2.2%	HS 376	IJ
20150424	13431	ANIK D-1	GPS Zero Phase, Inconel, Solar Cell Poly, Solar Cell MT, white paint, Aluminum	1.4%	HS 376	IJ
20150325	14234	TELSTAR 301	Anodized Aluminum, Exposed White Paint, Solar 15, S13 on al, Zero Phase GPS, White Paint, Inconel	1.7%	HS 376	just HK
20150325	14234	TELSTAR 301	Al 1100, Solar Cell CP, GPS Zero Phase, white paint, Solar Cell MT, Inconel	2.1%	HS 376	just IJ file
20150326	14234	TELSTAR 301	Anodized Alum, GPS Zero Phase, GPS 15, Solar Cell MT, Kapton	1.3%	HS 376	just HK
20150326	14234	TELSTAR 301	AL 1100, Inconel, GPS 15, Solar Cell CP, GPS Zero phase	2.1%	HS 376	just IJ
20150409	14234	TELSTAR 301	Anodized Aluminum, Solar Cell MT, Kapton (ITO), Exposed White Paint, Aluminum	1.0%	HS 376	just HK
20150425	14341	SL-4 DEBRIS	GPS Zero Phase, Inconel, Solar Cell MT, Aluminum	2.5%	debris	IJ
20150416	15383	ARABSAT 1-D (ANIK D-2)	Solar 15, AL 6061, Solar Cell MT , Solar Cell CP, GPS Zero Phase, Exposed White Paint, Inconel	1.3%	HS 376	HK

20150416	15383	ARABSAT 1-D (ANIK D-2)	Inconel, Solar 15, AL 1100, Solar Cell MT, Kapton (ITO), Kapton	2.5%	HS 376	IJ
20150420	15385	SPACENET1	Anodized Aluminum, GPS Zero Phase, Solar Cell MT, White Paint, Solar 15, Beta Cloth	1.5%	AS-3000	HK
20150420	15385	SPACENET1	White Paint, GPS Zero Phase, Kapton (AL), Inconel, Anodized Aluminum	2.1%	AS-3000	JH
20150410	16274	MORELOS 2	Kapton, GPS 15, ITO kapton, Solar Cell MT, inconel, AL 1100	1.8%	HS 376	just IJ file
20150410	16274	MORELOS 2	GPS 15, Kapton	3.4%	HS 376	just JH file
20150411	16274	MORELOS 2	Anodized Aluminum, Aluminum, GPS Zero Phase, Solar Cell MT, Inconel, Exposed White Paint, ITO Kapton	1.4%	HS 376	
20150411	16274	MORELOS 2	Kapton, GPS Zero Phase, Inconel, Solar 15	6.6%	HS 376	
20150416	16274	MORELOS 2	Anodized Aluminum, Solar 15, GPS Zero Phase, Exposed White Paint, White Paint, Kapton ITO	0.01%	HS 376	HK
20150416	16274	MORELOS 2	White Paint, Kapton ITO, Inconel, Solar 15, Solar Cell MT and CP, and Aluminum	1.2%	HS 376	IJ
20150424	16274	MORELOS 2	Anodized Aluminum, GPS Zero Phase, Solar 15, Solar MT, Exposed white paint, white paint	0.008%	HS 376	HK
20150425	16274	MORELOS 2	White Paint, GPS Zero Phase, Aluminum, Inconel, Kapton	1.1%	HS 376	just JH file
20150427	16274	MORELOS 2	White Paint, Inconel, GPS Zero Phase, Aluminum, Solar MT, Solar Poly, Solar 15	1.2%	HS 376	IJ
20150420	19751	COSMOS 1989 (ETALON 1)	Kapton H, Al 1100, S13 on Al, Beta cloth	2.6%	satellite	IJ
20150420	19751	COSMOS 1989 (ETALON 1)	Solar 15, Kapton (AL)	3.1%	satellite	JH
20150416	20026	COSMOS 2024 (ETALON 2)	Kapton ITO, Kapton, Solar Cell MT, Solar 15	3.3%	satellite	IJ
20150416	20026	COSMOS 2024 (ETALON 2)	Solar 15, Al 6061, Kapton, Inconel, Solar CP and MT, AL 1100	1.6%	satellite	JH
20150420	20558	ASIASAT 1	Anodized Aluminum, GPS Zero Phase, White Paint, Solar Cell MT, Solar 15, Beta Cloth, Inconel	0.1%	HS 376	HK
20150420	20558	ASIASAT 1	Inconel, AL 1100, Solar 15, Solar MT, Kapton ITO	1.7%	HS 376	IJ
20150413	20570	NEWSAT-1 (PALAPA B2R)	GPS Zero Phase Solar Cell, Inconel, Solar Cell MT, Kapton, Aluminum	2.3%	HS 376	IJ
20150413	20570	NEWSAT-1 (PALAPA B2R)	GPS Zero Phase Solar Cell, Al 1100, Inconel, Kapton, White Paint	2.5%	HS 376	JH
20150416	20570	NEWSAT-1 (PALAPA B2R)	Anodized Aluminum, GPS Zero Phase, Solar 15, Exposed White Paint, Inconel, Al, Kapton ITO	1.7%	HS 376	HK
20150416	20570	NEWSAT-1 (PALAPA B2R)	Inconel, GPS Zero Phase, AL 1100, Solar Cell MT, Solar 15, Solar Cell CP, White paint	1.8%	HS 376	IJ
20150412	21648	COSMOS 2054 Debris	Aluminum, less than 1% of Solar Poly, Solar 15	10.6%	debris	IJ

20150324	23185	APSTAR1	GPS Zero Phase Solar Cell, Anodized Aluminum, White Paint, Solar 15, Solar MT	1.3%	HS 376	just HK file
20150325	23185	APSTAR1	AL 1100, GPS 15, Solar Cell MT, Inconel, AL 6061, Kapton	1.3%	HS 376	just IJ
20150325	23185	APSTAR1	White paint, GPS zero phase, Aluminum Kapton, inconel	2.6%	HS 376	just JH
20150409	23185	APSTAR1	Kapton, Zero Phase GPS, Solar 15, Aluminum	2.0%	HS 376	just IJ
20150417	23615	IUS R/B(2)	Inconel, Al 1100, GPS Zero Phase, Kapton (AL), Solar Cell MT	3.2%	HS 376	IJ
20150417	23615	IUS R/B(2)	GPS Zero Phase, Anodized Aluminum, Inconel, Kapton (AL)	5.2%	HS 376	JH
20150420	23615	IUS R/B(2)	Exposed White Paint, Solar Cell MT, Kapton ITO, Inconel, Anodized Aluminum	2.7%	HS 376	HK
20150420	23615	IUS R/B(2)	GPS Zero Phase, Kapton (AL), Inconel, White Paint	3.8%	HS 376	JH
20150323	27400	ASTRA 3A	Solar Cell MT, Anodized Aluminum	5.5%	HS 376	HK
20150323	27400	ASTRA 3A	s13 on Aluminum	43.0%	HS 376	IJ
20150324	27400	ASTRA 3A	Anodized Aluminum, Solar Cell MT, GPS Zero Phase Solar Cell, Solar Cell Poly, Inconel	2.2%	HS 376	just JH file
20150410	27400	ASTRA 3A	Solar Cell MT, GPS Zero Phase, Anodized Aluminum	3.6%	HS 376	just HK
20150410	27400	ASTRA 3A	Solar Cell MT, GPS Zero Phase, Anodized Aluminum	3.6%	HS 376	just HK file
20150410	27400	ASTRA 3A	Anodized Aluminum, White paint, Kapton, GPS zero phase, S13 on al	1.6%	HS 376	just IJ
20150410	27400	ASTRA 3A	Anodized Aluminum, White Paint, Al Kapton, GPS Zero Phase, S13 on Al	1.6%	HS 376	just IJ file
20150412	27400	ASTRA 3A	GPS Zero Phase, Kapton (AL), inconel, White Paint	7.8%	HS 376	HK
20150424	27400	ASTRA 3A	Solar Cell MT, GPS Zero Phase, Anodized Aluminum	3.6%	HS 376	HK
20150424	27400	ASTRA 3A	Kapton (AL), Beta Cloth, White Paint, Solar Cell CP, Solar 15	4.2%	HS 376	IJ
20150426	27400	ASTRA 3A	Solar Cell MT, Anodized Aluminum	6.5%	HS 376	JH
20150320	39866	SL-16 DEBRIS	Kapton, Anodized Aluminum, White Paint	7.0%	Debris	
20150321	39886	SL-16 DEBRIS	s13 on Aluminum	7.0%	Debris	IJ